Consistent Landmark and Intensity-based Image Registration

Hans J. Johnson and Gary E. Christensen

Department of Electrical and Computer Engineering
The University of Iowa, Iowa City, IA, 52242, USA

Correspondence:

Gary E. Christensen, D.Sc.
Department of Electrical and Computer Engineering
The University of Iowa
4016 SC
Iowa City, IA 52242
Tel. (319) 335-6055
FAX: (319) 335-6028
E-mail: gary-christensen@uiowa.edu

Abstract

Two new consistent image registration algorithms are presented: one is based on matching corresponding landmarks and the other is based on matching both landmark and intensity information. The consistent landmark and intensity registration algorithm produces good correspondences between images near landmark locations by matching corresponding landmarks and away from landmark locations by matching the image intensities. In contrast to similar unidirectional algorithms, these new consistent algorithms jointly estimate the forward and reverse transformation between two images while minimizing the inverse consistency error—the error between the forward (reverse) transformation and the inverse of the the reverse (forward) transformation. This reduces the ambiguous correspondence between the forward and reverse transformations associated with large inverse consistency errors. In both algorithms a thin-plate spline model is used to regularize the estimated transformations. Examples are presented that show the inverse consistency error produced by the traditional unidirectional landmark thin-plate spline algorithm can be relatively large and that this error is minimized using the consistent landmark algorithm. Results using MRI data are presented that demonstrate that using landmark and intensity information together produce better correspondence between medical images than using either landmarks or intensity information alone.

Keywords: image registration, correspondence, inverse transformation, deformable templates, landmark registration,

1 Introduction

There are many image registration algorithms based on the exact matching of corresponding landmarks in two images [7]. The unidirectional landmark thin-plate spline image (UL-TPS) registration technique pioneered by Fred Bookstein [1, 4, 2] is the most commonly used landmark driven image registration algorithm. Generalizations of UL-TPS procedure include Krieging methods [14, 13] that use regularization models other than

the thin-plate spline (TPS) model, anisotropic landmark interactions [16], and directed landmarks [3].

Most landmark based registration algorithms, including the ones described in this paper, assume that a small deformation is sufficient to register a set of images. In cases where the small deformation assumption holds, registration algorithms may efficiently estimate diffeomorphic transformations in a solution space that contain non-diffeomorphic transformations. The small deformation limitation is not universally applicable, and work by Joshi et. al.[11, 15, 12] estimates large deformation transformations in a solution space of diffeomorphisms by constraining the transformations to obey diffeomorphic fluid properties.

The UL-TPS algorithm (see Section 2.2) defines a unique smooth registration from a template image to a target image based on registering corresponding landmarks. Correspondence away from the landmark points is defined by interpolating the transformation with a thin-plate spline model. Although thin-plate spline interpolation produces a smooth transformation from one image to another, it does not define a consistent correspondence between the two images except at the landmark points. This can be seen by comparing the transformation generated by matching a set of template landmarks to a set of target landmarks with the transformation generated by matching the target landmarks to the template landmarks. If the correspondence is consistent then the forward and reverse transformations will be inverses of one another. This is not the case as shown by the examples in Section 3.

In this paper, the idea of consistent image registration [5, 10, 6] is combined with the thin-plate spline algorithm [1, 4, 2, 8, 16] to overcome the problem that the forward and reverse transformations generated by the thin-plate spline algorithm are not inverses of one another. In the consistent image registration approach, the forward and reverse transformations between two images are jointly estimated subject to the constraints that they minimize the thin-plate spline bending energy and that they are inverses of one another. The merger of these two approaches produced a landmark-based consistent thin-plate spline (CL-TPS) and a landmark and intensity-based consistent thin-plate spline (CLI-

TPS) image registration algorithms. The CL-TPS algorithm (see Section 2.3) provides a means to estimate a consistent pair of forward and reverse transformations given a set of corresponding points. The CLI-TPS algorithm (see Section 2.1) combines both landmark and intensity information to estimate a consistent pair of forward and reverse transformations.

2 Methods

2.1 Consistent Landmark and Intensity-based Registration

The consistent landmark and intensity image registration algorithm is outlined in Fig. 1. It is assumed that the images being registered have been rigidly rotated and translated to put them into a standard orientation, such as the Talairach coordinate system[17], before applying this procedure. The first step of the algorithm is to produce a good initial nonrigid registration using a landmark initialization step. This step consists of (1) picking corresponding landmarks in the two images, (2) solving the unidirectional TPS algorithm modified to produce periodic boundary conditions for the forward and reverse transformations, and (3) averaging the forward transformation with the inverse of the reverse transformation, and vice versa. The full details of the landmark initialization are described in Section 2.2.

After the landmark initialization step, the iterative consistent landmark thin-plate spline algorithm described in Section 2.3 is used to produce a consistent set of forward and reverse transformations. This algorithm jointly estimates a set of transformations that minimize both the inverse consistency error and the bending energy of the thin-plate spline model while maintaining exact correspondence at the landmarks. The resulting forward and reverse transformations have orders of magnitude less inverse consistency error than the original unidirectional TPS transformations as shown by the experiments in the Results Section.

The last step of the algorithm is to use the consistent intensity registration algorithm[5, 10, 6], that is briefly described in Appendix B, to refine the transformations based on

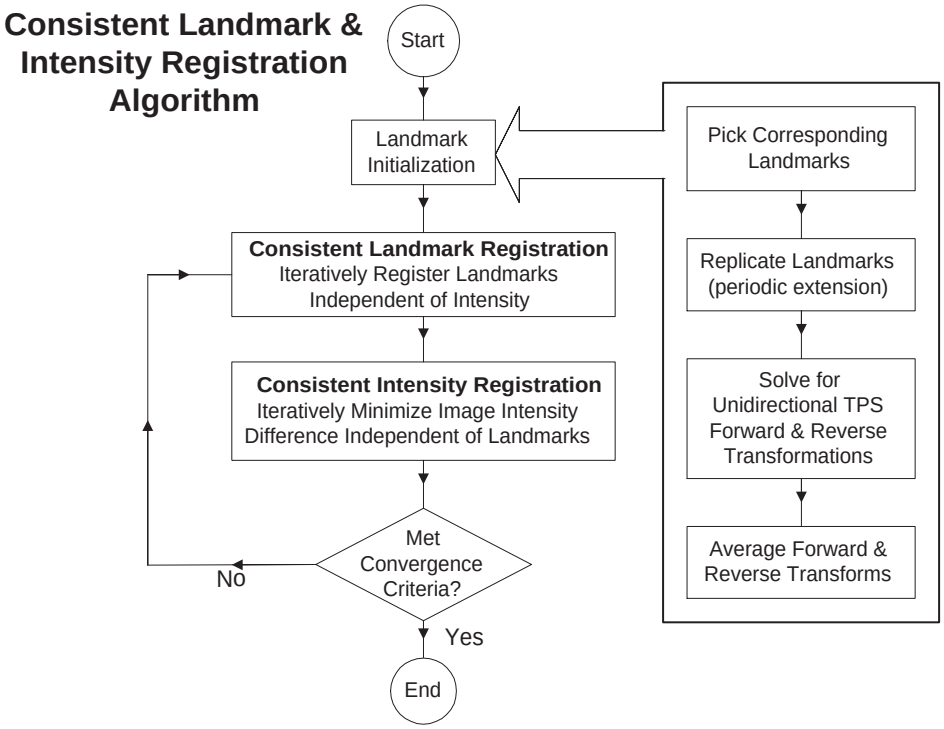

Figure 1: Flow chart describing the steps of the Consistent Landmark and Intensity Image Registration algorithm. The images being registered are assumed to be rigidly aligned before starting this procedure.

matching the intensities of the images. This step matches the images in regions away from the landmarks by minimizing the intensity differences in these regions. The intensity matching does little in regions near corresponding landmarks since these regions have similar intensity patterns that have all ready been matched by the landmark registration. During the intensity matching step, the landmark correspondence error increases in regions where there are bad landmark initializations. The landmark correspondence error also increases in this step due to the TPS regularization model that can pull corresponding landmarks apart. The landmark registration error can be minimized by applying the consistent landmark registration step followed again by the intensity registration step.

The process of alternating between matching the landmarks and then the image intensities is repeated until an appropriate stopping criteria is met. In this work, a fixed number of iterations was used as the stopping criteria. Alternatively, the algorithm could

be stopped after an acceptable intensity similarity and landmark error cost is achieved. The optimal strategy for stopping the algorithm can be quite complex and will be studied in future work.

The consistent landmark and intensity-based TPS algorithm can be thought of as estimating a consistent set of forward and reverse transformations that minimize the intensity differences between two images while being guided by the landmark correspondences. The landmarks guide the solution by initializing the consistent intensity registration algorithm with transformations that are nearly inverse consistent and have exact correspondence at the landmarks. This initialization helps the consistent intensity registration avoid some local minima and therefore produce more biologically relevant correspondence maps.

Due to the difficulty of defining exact landmark correspondences, the final solution is determined from the intensity information alone. The choice not to use the landmarks for the final registration can be justified by the fact that the landmarks are selected from the intensity data and are therefore implicitly contained in the intensity data.

The following notation will be used throughout the rest of the paper. The variables q_i and p_i, for $i = 1, \ldots, M$, denote the M corresponding landmarks in the template T and target S images, respectively. The domain of the template image T and target image S is denoted by Ω. The forward transformation $h : \Omega \to \Omega$ is defined as the mapping that transforms T into the shape of S and the reverse transformation $g : \Omega \to \Omega$ is defined as the mapping that transforms S into the shape of T. The forward and reverse displacement displacement fields are defined as $u(x) = h(x) - x$ and $w(x) = g(x) - x$, respectively. The inverse of the forward and reverse transformations denoted by $h^{-1}(x)$ and $g^{-1}(x)$, respectively, can be expressed in terms of the displacement fields $\tilde{u}(x) = h^{-1}(x) - x$ and $\tilde{w}(x) = g^{-1}(x) - x$, respectively.

2.2 Unidirectional Landmark Thin-Plate Spline Registration

The unidirectional landmark-based, thin-plate spline (UL-TPS) image registration algorithm [1, 4, 2] registers a template image $T(x)$ with a target image $S(x)$ by matching corresponding landmarks identified in both images. Registration at non-landmark points

is accomplished by interpolation such that the overall transformation smoothly maps the template into the shape of the target image.

The unidirectional landmark image registration problem can be thought of as a Dirichlet problem [13] and can be stated mathematically as finding the displacement field u that minimizes the cost function

$$C = \int_{\Omega} ||\mathcal{L}u(x)||^2 dx \tag{1}$$

subject to the constraints that $u(p_i) = q_i - p_i$ for $i = 1, \ldots, M$. The operator $\mathcal{L}$ denotes a symmetric linear differential operator [9] and is used to interpolate u away from the corresponding landmarks. When $\mathcal{L} = \nabla^2$, the problem reduces to the thin-plate spline image registration problem given by

$$C = \int_{\Omega} ||\nabla^2 u(x)||^2 dx = \sum_{i=1}^{2} \int_{\Omega} \left(\frac{\partial^2 u_i(x)}{\partial^2 x_1} \right)^2 + 2 \left(\frac{\partial^2 u_i(x)}{\partial x_1 \partial x_2} \right) + \left(\frac{\partial^2 u_i(x)}{\partial^2 x_2} \right)^2 dx_1 dx_2 \tag{2}$$

subject to the constraints that $u(p_i) = q_i - p_i$ for $i = 1, \ldots, M$.

It is well known [1, 4, 2] that the thin-plate spline displacement field $u(x)$ that minimizes the bending energy defined by Eq. 2 has the form

$$u(x) = \sum_{i=1}^{M} \xi_i \phi(x - p_i) + Ax + b. \tag{3}$$

where $\phi(r) = r^2 \log r$ and ξ_i are 2×1 weighting vectors. The 2×2 matrix $A = [a_1, a_2]$ and the 2×1 vector b define the affine transformation where a_1 and a_2 are 2×1 vectors. The procedure used to determine these unknown constants is described in Appendix A.

The thin-plate spline interpolant $\phi(r) = r^2 \log r$ is derived assuming infinite boundary conditions, i.e., Ω is assumed to be the whole plane R^2. The thin-plate spline transformation is truncated at the image boundary when it is applied to an image. This presents a mismatch in boundary conditions at the image edges when comparing forward and reverse transformations between two images. It also implies that a thin-plate spline transformation is not a one-to-one and onto mapping between two image spaces. To overcome

this problem and to match the periodic boundary conditions assumed by the intensity-based consistent image registration algorithm [5, 6], we use the following procedure to approximate periodic boundary conditions for the thin-plate spline algorithm.

Figure 2 illustrates the concept of periodic boundary conditions for the landmark thin-plate spline registration problem. Cyclic boundary conditions implies a toroidal coordinate system such that the left-right and top-bottom boundaries of the domain Ω are mapped together. Modifying the boundary conditions in this manner causes an infinite number of interactions between landmarks for a given finite set of landmark points. Panel (b) shows two such interactions between landmark points p_1 and p_2; one within the domain Ω and another between adjacent image domains. We approximate the solution of Laplace's Equation with periodic boundary conditions by solving the TPS registration problem with replicated the landmark locations in the eight adjacent domains as shown in panel (b) of Fig. 2. This provides a good approximation to periodic boundary conditions since the the kernel function, $\phi(r) = r^2 \log r$, causes interactions between landmarks to decrease rapidly as the distance between landmarks increases. In our tests, there were differences

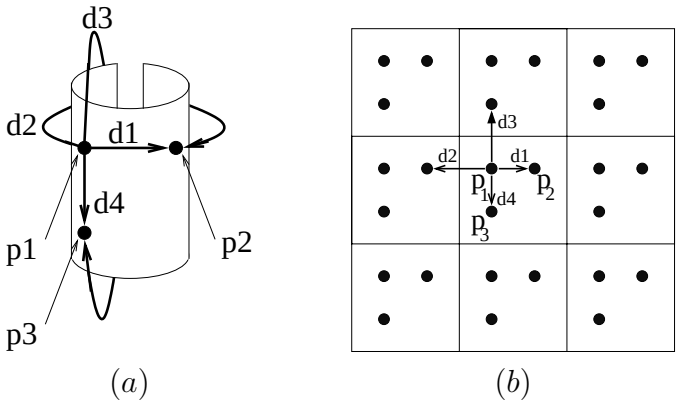

Figure 2: Diagrams describing the coordinate system and points used to ensure that the resulting displacement field demonstrates continuous periodic boundary conditions. The left panel is a depiction of the toroidal coordinate system. The right panel shows the layout of the point used to solve the thin-plate spline with approximate circular boundaries.

between the transformations found using infinite and periodic boundary conditions but there was nearly no difference in terms of the magnitude of the fiducial landmark errors.

The major differences between the two sets of boundary conditions was in the location of the maximum inverse consistency error. The maximum inverse consistency error was located on the image boundaries in the case of infinite boundary conditions while it was away from the boundaries for the case of periodic boundary conditions.

The inverse consistency error of the forward and reverse transformations generated by the UL-TPS can be made smaller by averaging the forward transformation with the inverse of the reverse transformation. This averaging will be referred to as the averaged unidirectional landmark-based thin-plate spline (AUL-TPS) algorithm and is used to initialize the consistent landmark TPS algorithm described in the next section. Note that this procedure does not significantly effect the fiducial error at the landmarks since the displacement at the landmark locations in the forward, reverse, inverse-forward, and inverse-reverse transformations are nearly zero as computed by the UL-TPS algorithm.

2.3 Consistent Landmark Thin-Plate Spline Registration

The averaged unidirectional landmark-based thin-plate spline (AUL-TPS) image registration algorithm produces consistent correspondence only at the landmark locations. The consistent landmark-based, thin-plate spline (CL-TPS) image registration algorithm is designed to align the landmark points and minimize the consistency errors across the entire image domain.

The CL-TPS algorithm is solved by minimizing the cost function given by

$$\begin{aligned} C &= \rho \int_\Omega ||\mathcal{L}u(x)||^2 + ||\mathcal{L}w(x)||^2 dx \\ &+ \chi \int_\Omega ||u(x) - \tilde{w}(x)||^2 + ||w(x) - \tilde{u}(x)||^2 dx \\ &\quad \text{subject to } p_i + u(p_i) = q_i \text{ for } i = 1, \ldots, M. \end{aligned} \tag{4}$$

The first integral of the cost function defines the bending energy of the thin-plate spline for the displacement fields u and w associated with the forward and reverse transformations, respectively. This term penalizes large derivatives of the displacement fields and provides the smooth interpolation away from the landmarks. The second integral is called

the inverse consistency constraint (ICC) and is minimized when the forward and reverse transformations are inverses of one another. This integral couples the estimation of the forward and reverse transformations together and penalizes transformations that are not inverses of one another. The constants ρ and χ define the relative importance of the bending energy minimization and the inverse consistency terms of the cost function. Notice that this problem is a nonlinear minimization problem since the inverse consistency constraint is a function of the inverse-forward $h^{-1}(x) = x+\tilde{u}(x)$ and inverse-reverse $g^{-1}(x) = x+\tilde{w}(x)$ transformations.

Equation 4 is minimized numerically using the CL-TPS algorithm described in Figure 3. The algorithm is initialized with the forward and reverse displacement fields u and w either set to zero as in Figure 3 or with the result of a previous registration algorithm. The temporary variables r_l and s_l are initially set equal to the landmark locations q_l and p_l, respectively, for $l = 1, \ldots M$. The value of r_l converges from q_l to p_l as the algorithm converges, and in similar fashion, the value of s_l converges from p_l to q_l.

At each iteration of the algorithm, the unidirectional landmark thin-plate spline (UL-TPS) algorithm with periodic boundary conditions is used to solve for the perturbation field f_1 that minimizes the distance between the current position of r_l and its final position p_l. The perturbation field f_1 times the step size α is added to the current estimate of the forward displacement field u where α is a positive number less than one. This procedure is repeated to update the reverse displacement field w. Next, the forward displacement field u is updated with the step size β times the gradient of the inverse consistency constraint with respect to u assuming that $\tilde{w}$ is constant. The displacement field $\tilde{w}$ is computed by taking the inverse of the transformation $g(x) = x+w(x)$ as described in our previous paper describing the consistent intensity registration algorithm [6]. This step is repeated in the reverse direction to update the displacement field $w(x)$. These steps are repeated until the landmark error and the inverse consistency error fall below problem specific thresholds or until a specified number of iterations are reached. In practice, this algorithm converges to an acceptable solution within five to ten iterations and therefore we use a maximum number of iterations as our stopping criteria.

Consistent Landmark Thin-plate Spline (CL-TPS) Registration Algorithm

1. Initialization: Set $u(x) = 0$, $w(x) = 0$, $r_l = q_l$, and $s_l = p_l$.
2. Compute $f_1(x)$ that satisfies $\nabla^4 f_1(x) = 0$ subject to $f_1(r_l) = p_l - r_l \quad \forall l$ using the periodic boundary UL-TPS algorithm.
3. Compute $f_2(x)$ that satisfies $\nabla^4 f_2(x) = 0$ subject to $f_2(s_l) = q_l - s_l \quad \forall l$ using the periodic boundary UL-TPS algorithm.
4. Set $u(x) = u(x) + \alpha f_1(x)$ and $w(x) = w(x) + \alpha f_2(x)$.
5. Set $r_l = q_l + u(r_l)$ and $s_l = p_l + w(s_l)$.
6. Compute h^{-1} and g^{-1} using procedure described in [6].
7. Set $\tilde{u}(x) = h^{-1}(x) - x$ and $\tilde{w}(x) = g^{-1}(x) - x$.
8. Set $u(x) = u(x) + \beta[u(x) - \tilde{w}(x)]$ and $w(x) = w(x) + \beta[w(x) - \tilde{u}(x)]$.
9. If the maximum landmark error $|u(q_l) - (p_l - q_l)|$ or $|w(p_l) - (q_l - p_l)|$ is greater than a threshold ϵ_1 or the maximum inverse consistency error $|u(x) - \tilde{w}(x)|$ or $|w(x) - \tilde{u}(x)|$ is greater than a threshold ϵ_2 then Goto 2.

Figure 3: Consistent Landmark Thin-plate Spline (CL-TPS) Registration Algorithm

2.4 Appending the Consistent Landmark and Intensity Registration Algorithms

The parameterization of the transformations used in the consistent landmark (CL-TPS) algorithm and the consistent intensity (CI-TPS) algorithm are different. A spatial sampling parameterization of the displacement field is used in the CL-TPS algorithm while a Fourier series parameterization of the displacement field is used in the CI-TPS algorithm. The parameterization used in one algorithm must be converted into the parameterization of the other in order to use the result from one algorithm to initialize the other as outlined in the CLI-TPS algorithm defined in Fig. 1. This is accomplished by using the Fast Fourier Transform (FFT) and the Inverse Fast Fourier Transform (IFFT) to convert the spatial representation of the displacement field to the Fourier Series representation and vica versa.

3 Results

3.1 Landmark Registration

The first experiment compares the inverse consistency error associated with the traditional unidirectional landmark thin-plate spline (UL-TPS) algorithm to that of the consistent landmark thin-plate spline (CL-TPS) algorithm. This simple experiment is designed to show that the UL-TPS algorithm can have significant inverse consistency error while this error is minimized using the CL-TPS algorithm. The experiment shown in Fig. 4 consisted of matching eight landmarks in one image to their corresponding landmarks in a second image using both the UL-TPS and the CL-TPS algorithm. The arrows in the first and second panels show the displacement between the corresponding landmarks in the forward and reverse directions, respectively. The four landmarks in the corners of the images were fixed. The forward transformation h maps the four inner points to the four outer points and the reverse transformation g maps the outer points to the inner points. Applying the CL-TPS transformations to a rectangular grid shows that the forward transformation—

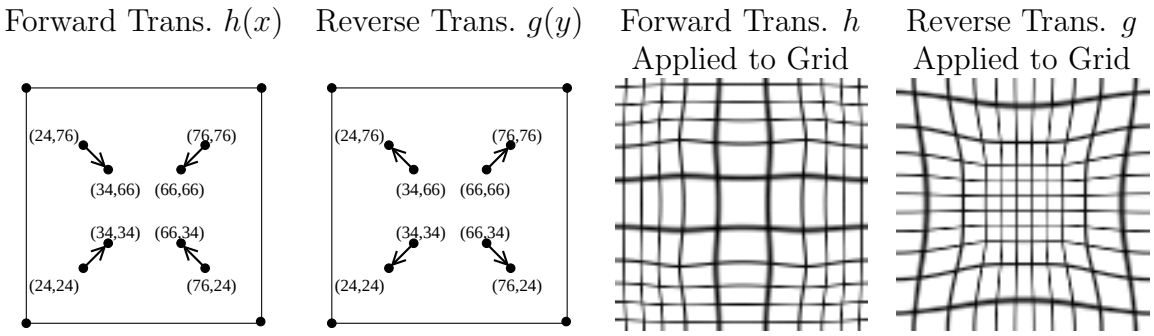

Figure 4: The location of local displacements at the landmarks points for the forward, and reverse transformations of images with 100×100 pixels. Application of the thin-plate spline deformation fields to uniformly spaced grids for the forward and reverse transformations.

defined with respect to a Eulerian frame of reference—causes the center of the image to expand (third panel of Fig. 4) while the reverse transformation causes a contraction of the central portion of the image (fourth panel of Fig. 4).

The top row of Fig. 5 shows the spatial locations and magnitudes of the inverse consistency errors of the forward and reverse transformations generated by the UL-TPS algorithm. The images in the left column were computed by taking the Euclidean norm of the difference between the forward transformation h and the inverse of the reverse transformation g^{-1}. The images in the center column were computed in a similar fashion with g and h^{-1}. The CL-TPS result was created using AUL-TPS initialization and minimizing for 100 iterations with $\alpha = 0.5$ and $\beta = 0.012$. This registration took approximately 3 minutes on a single 667MHz alpha processor.

The tables in Fig. 5 tabulate the inverse consistency error at four representative points in the images. The points A and C are located at points away from landmarks while the points B and D are located at landmark locations. The inverse consistency error at the landmark points is small for both algorithms. However, the landmark error is quite large away from the landmark locations in the UL-TPS algorithm. The range of intensities on the color bar for each method shows that the range of inverse consistency errors for the UL-TPS algorithm was in the range of 0.002 to 4.9 pixels while this same error for the CL-TPS algorithm ranged from 0.00 to 0.009. This shows that the CL-TPS

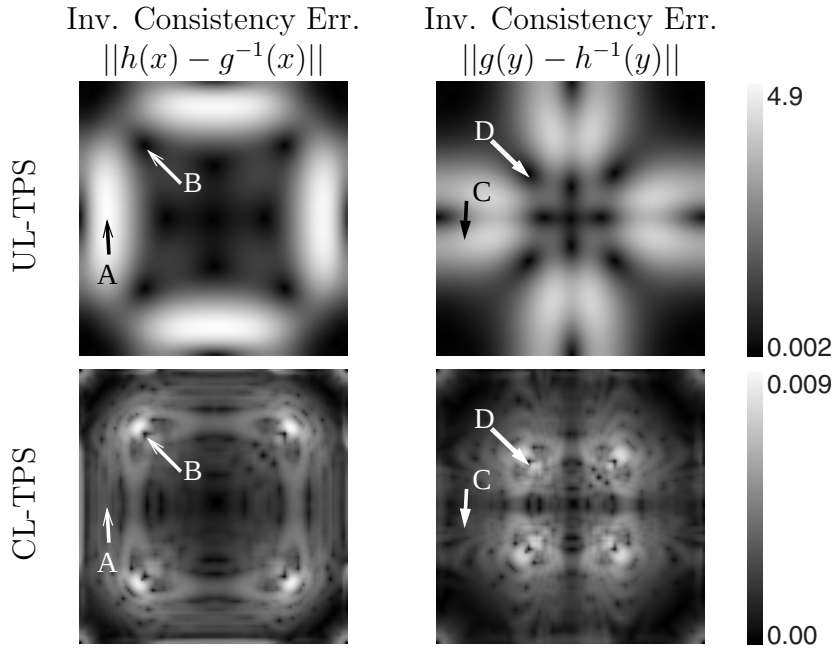

Inv. Consistency Err.

UL-TPS		
Label	Point	Pixel Err.
A	(10,50)	4.9
B	(24,76)	0.0073
C	(20,40)	3.9
D	(34,66)	0.0060

CL-TPS		
Label	Point	Pixel Err.
A	(10,50)	0.0030
B	(24,76)	0.000064
C	(20,40)	0.0034
D	(34,66)	0.000081

Figure 5: The left and center panels show the inverse consistency errors of the forward and reverse transformations, respectively. The tables in the right columns list the fiducial errors associated with selected image points. The top and bottom rows are the inverse consistency errors associated with the unidirectional (UL-TPS) and consistent (CL-TPS) landmark thin-plate spline algorithms, respectively.

algorithm reduced the inverse consistency error by over 500 times that of the UL-TPS algorithm for this example. A pair of transformations are point-wise consistent if the composite function $h(g(x))$ maps a point x to itself. Spatial deviations from the identity mapping can be visualized by applying the composite mapping to a uniformly spaced grid. The grid is deformed by the composite transformation in regions where the forward and reverse transformations have inverse consistency errors. The composite transformation does not deform the grid for a perfectly inverse consistent set of forward and reverse transformations. Fig. 6 shows the composite mapping produced by the UL-TPS (left) and the CL-TPS (right) applied to a rectangular grid for this experiment. Notice that there is a considerable amount of inverse consistency error in the UL-TPS algorithm while there is no visually detectable inverse consistency error produced by the CL-TPS algorithm.

The minimum and maximum Jacobian values of the forward (reverse) transforma-

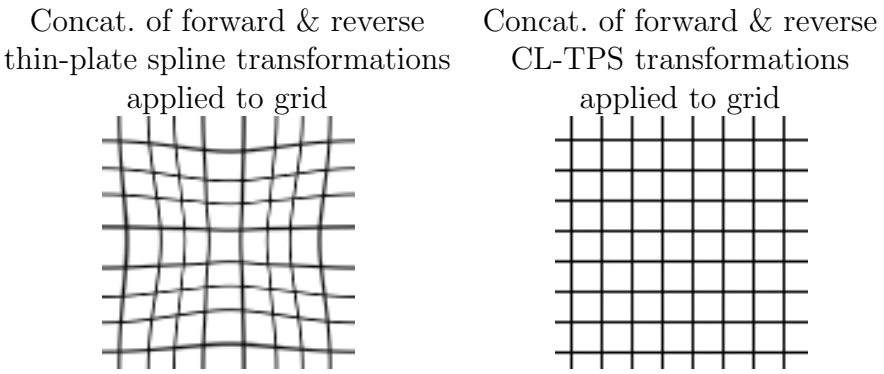

Figure 6: Deformed grids showing the error between the forward and reverse transformations estimated with the landmark-based thin-plate spline algorithm(left panel) and the CL-TPS algorithm(right panel). The grids were deformed by the transformation constructed by composing the forward and reverse transformations together, i.e., $g(h(x))$. Ideally, the composition of the forward and reverse transformations is the identity mapping which produces no distortion of the grid as in the right panel.

tion specify the maximum expansion and contraction of the transformation, respectively. The Jacobian error, calculated as $\frac{1}{2}|min\{Jac(h)\} - 1/max\{Jac(g)\}| + \frac{1}{2}|min\{Jac(g)\} - 1/max\{Jac(h)\}|$, provides an indirect measure of the inconsistency between the forward and reverse transformations. The Jacobian error is zero if the forward and reverse transformations are inverses of one another, but the converse is not true. Notice that the Jacobian error was 1000 times smaller for the CL-TPS algorithm compared to the UL-TPS algorithm.

3.2 Landmark and Intensity Registration

The five 2D transverse MRI data sets shown in Fig. 7 were used to compare the performance of the unidirectional landmark (UL-TPS); consistent landmark (CL-TPS); consistent intensity (CI-TPS); and consistent landmark and intensity (CLI-TPS) thin-plate spline algorithms. These 256×320 pixel images with 1 millimeter isotropic pixel dimension were extracted from 3D MRI data sets such that they roughly corresponded to one another. A set 39 of corresponding landmarks were manually defined in data sets two and four and a subset of the 39 landmarks were manually defined in the additional 3 data-sets

Table 1: Comparison between the unidirectional (UL-TPS), averaged unidirectional (AUL-TPS), and consistent (CL-TPS) thin-plate spline image registration algorithms. The table columns are the Experiment, (ICC), transformation Direction (TD), average fiducial error (AFE) in pixels, maximum fiducial error (MFE), maximum inverse error (MIE) in pixels, average inverse error (AIE) in pixels, minimum Jacobian value (MJ), inverse of the maximum Jacobian value (IJ), and the Jacobian error (JE).

Experiment	ICC	TD	AFE	MFE	AIE	MIE	MJ	IJ	JE
UL-TPS	No	Forward	0.010	0.016	2.2	4.1	2.4	4.8	1.4
		Reverse	0.0056	0.010	2.0	4.9	2.9	3.2	
AUL-TPS	No	Forward	0.0074	0.013	0.091	0.20	0.28	0.47	0.011
		Reverse	0.0072	0.012	0.082	0.29	0.45	0.27	
CL-TPS	Yes	Forward	0.00055	0.0011	0.0028	0.0078	0.28	0.48	0.0012
(100 iter.)		Reverse	0.00046	0.00094	0.0024	0.0088	0.48	0.28	

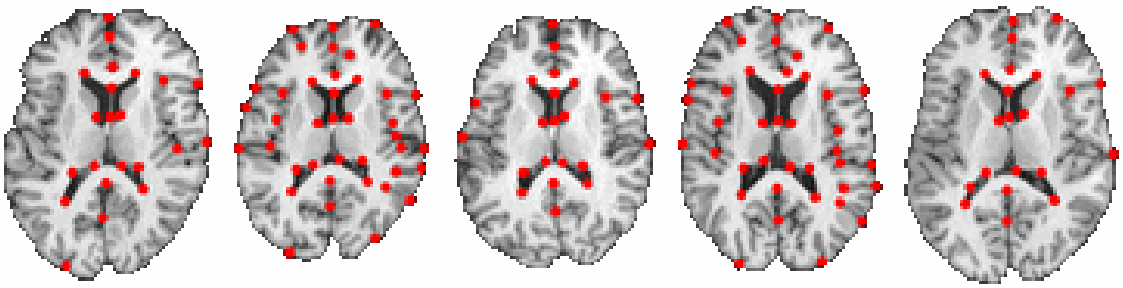

$B1$ $B2$ $B3$ $B4$ $B5$

Figure 7: Five corresponding image slices from MRI acquired brains with manually identified points of correspondence.

(see Fig. 7). Data set two was chosen as the template and was deformed into the shape of the other four data sets using all four registration algorithms. Only the landmarks that were defined in both the template and target data sets were used in the landmark-based algorithms. All four algorithms were initialized with the averaged unidirectional landmark thin-plate spline (AUL-TPS) registration algorithm defined in Section 2.2.

Table 2 lists the parameters used for each algorithm and the computation time that each algorithm required to run on a single 667MHz alpha processor. The algorithmic parameters were chosen to demonstrate the registration performance of the algorithms

Table 2: Summary of algorithm parameters and computation times on a single 667MHz alpha processor.

Algorithm	Iterations	Computation Time	χ	ρ	σ	α	β
UL-TPS	1	5 seconds	NA	NA	NA	NA	NA
CL-TPS	20	3 minutes	NA	NA	NA	1.0	0.0061
CI-TPS	1000	1 hour	500	0.0000075	0.10	NA	NA
CLI-TPS	300	1 hour	500	0.0000075	0.50	1.0	0.0061

independent of optimizing the run times. These computation times can be decreased significantly by optimizing the computer code and reducing the number of iterations. The CLI-TPS algorithm was run for 5 iterations of the CL-TPS registration algorithm followed by 95 iterations of the CI-TPS registration algorithm.

The result of transforming MRI data set $B5$ in to the shape of $B2$ using each of the four registration algorithms is shown in Fig. 8. These results are typical of the other pairwise registration combinations. The images are arranged left to right from the worst to the best similarity match as shown by the corresponding difference images shown below the transformed images. The UL-TPS and CL-TPS algorithms perform almost identically with respect to similarity matching. The CI-TPS and CLI-TPS intensity based registrations produce better similarity match than the two landmark only methods. In particular, the intensity based methods match the border locations and non-landmark locations better than the landmark thin-plate spline or CL-TPS algorithms.

The images in Fig. 9 show the Jacobian of the forward and reverse transformations between images $B2$ and $B1$ produced by the CL-TPS(left two panels) and CLI-TPS(right two panels) algorithms, respectively. The value of the Jacobian at a point is encoded such that bright pixels represent expansion, and dark pixels represent contractions. Notice that the intensity pattern of the forward and reverse Jacobian images appear nearly opposite of one another since expansion in one domain corresponds to contraction in the other domain. These images show the advantage of using both landmark and intensity information together as opposed to just using landmark information alone. Notice that the CL-TPS algorithm has very smooth Jacobian images compared to the CLI-TPS algo-

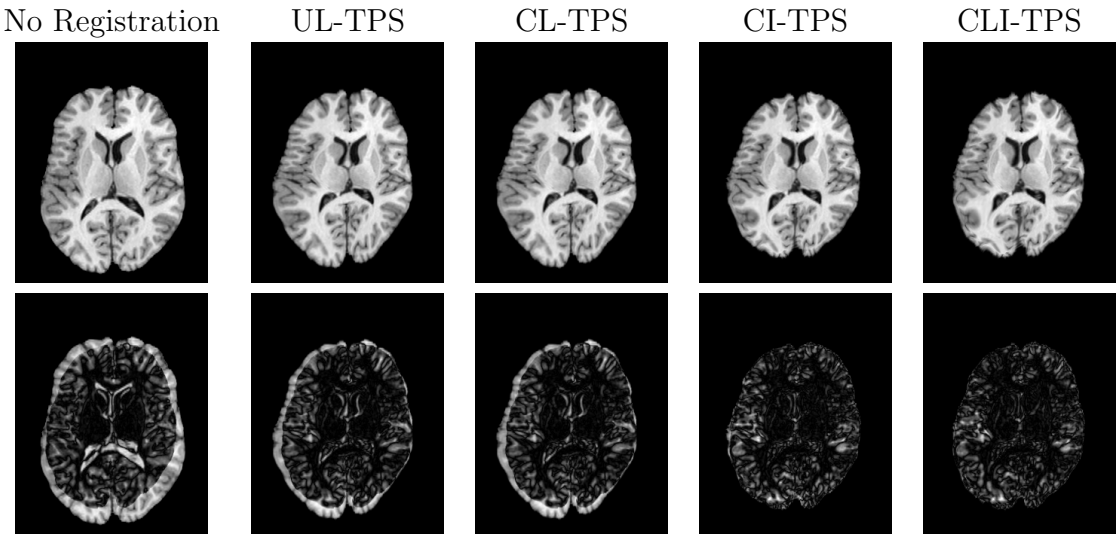

Figure 8: Intensity matching results for registering dataset $B5$ to dataset $B2$ with the four registration algorithms. The top row shows the data set $B5$ transformed into the shape of $B2$ using each algorithm and the bottom row shows the absolute difference image between the transformed $B5$ image and the target $B2$ image.

rithm. This is because the CL-TPS algorithm matches the images at the corresponding landmarks and smoothly interpolates the transformation between the landmarks. Conversely, the patterning of the local distortions in the CLI-TPS registration resemble the underlying intensity patterning. This indicates that combining the intensity information with the landmark information provides additional local deformation as compared to using the landmark information alone. This improved registration between landmarks produces more distortion of the template image and therefore there is a larger range of Jacobian values for the CLI-TPS algorithm than the CL-TPS algorithm as shown by the color bar scales.

Inverse consistency error images are computed by taking the Euclidean norm of the difference between the forward and the inverse of the reverse transformations at each voxel location in the image domain. Figure 10 shows the inverse consistency error images for the registration of data sets $B2$ and $B5$ using the UL-TPS, CL-TPS, CI-TPS, and and CLI-TPS algorithms. Note that each images is on its own color-scale and that the UL-TPS algorithm has 10 to 200 times more maximum inverse consistency error than

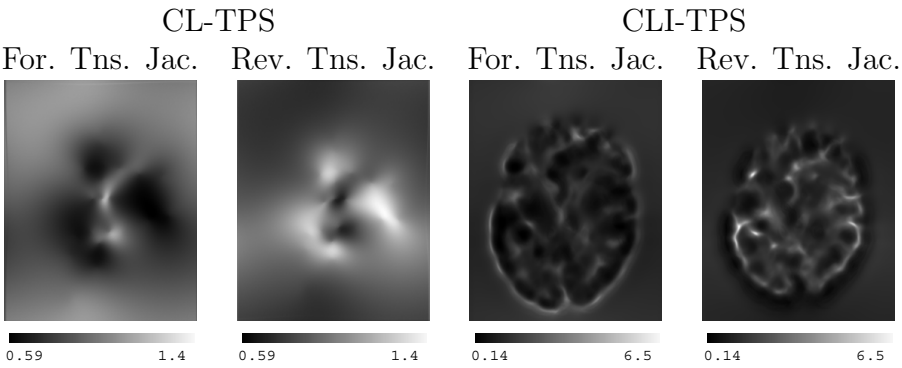

Figure 9: This figure shows the Jacobians of the forward and reverse transformations for the registration of data sets $B2$ and $B1$ for the CL-TPS(left two panels) and CLI-TPS(right two panels) algorithms. The bright pixels of the Jacobian images represent regions of expansion, and dark pixels represent regions of contraction.

the consistent registration algorithms. The UL-TPS algorithm had 50 to 500 times more average inverse consistency error than the consistent registrations algorithms. This can be seen by comparing large regions of bright pixels in the UL-TPS image to the small regions of bright pixels in the other images. This figure shows that consistent registration algorithms produced forward and reverse transformations that had sub-voxel inverse consistency errors at all voxel locations. The inverse consistent errors in the UL-TPS and CL-TPS algorithms are greatest away from the landmark driving forces because the landmark driving forces are implicitly inverse consistent. The largest inverse consistency errors in the CI-TPS and CLI-TPS algorithms occur near edges where there is a correspondence ambiguity associated with the intensity matching solution.

Fig. 11 shows plots of the intensity similarity cost, landmark error cost, and the maximum inverse consistency error costs as a function of iteration for CLI-TPS registration of data sets $B2$ and $B4$. The protocol used for this experiment was 5 iterations of the CL-TPS algorithm followed by 95 iterations of the CI-TPS algorithm. The intensity similarity cost decreases during the CI-TPS algorithm when the intensity is being matched and increases during the CL-TPS algorithm as the landmarks are matched. Conversely, the landmark error decreases during the CL-TPS algorithm and increases during CI-TPS algorithm as the intensity is matched. The plot of the maximum inverse consistency error

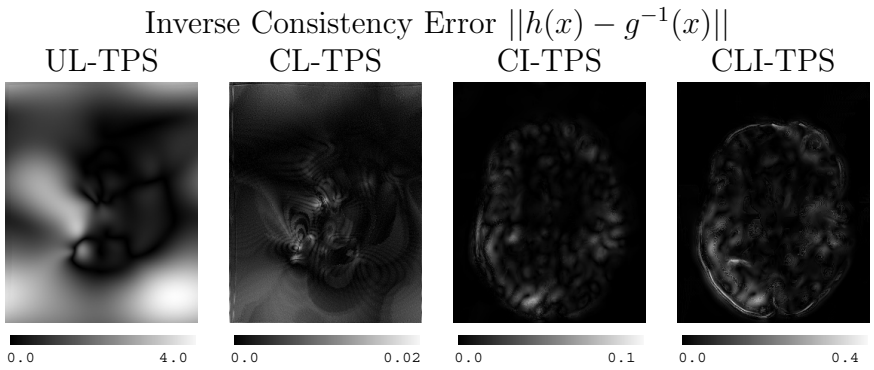

Figure 10: Images that display the magnitude and location of forward transformation inverse consistency errors for matching data sets $B2$ and $B5$ with UL-TPS, CL-TPS, CI-TPS, and CLI-TPS registration algorithms.

shows that switching from the intensity (CI-TPS) to the landmark (CL-TPS) algorithm causes a jump in the inverse consistency error which is quickly minimized. We observed that smaller landmark and intensity error is achieved by the CLI-TPS in one-third the number of iterations than by either CI-TPS or CL-TPS alone.

The lower-right panel of Fig. 11 shows the minimum and maximum Jacobian values of the forward and reverse transformations as a function of iteration. These plots show that the inverse consistency constraint (ICC) causes the minimum Jacobian value of the forward transformation to track with the inverse of the maximum Jacobian value of the reverse transformation and vice versa. Note that these plots give an upper bound on the inverse consistency error since the minimum and maximum Jacobian values of the forward and reverse transformations do not correspond to the same points.

Table 3 summarizes the representative statistics collected from the experiments. Comparing the results of the UL-TPS and CL-TPS algorithms shows that the addition of inverse consistency constraint (ICC) improved the inverse consistency of the transformations with no degradation of the fiducial landmark matching. Note that for the UL-TPS algorithm, the inverse consistency error tends to be be larger as one moves away from landmarks and that the inverse consistency error can be decreased by defining more corresponding landmarks.

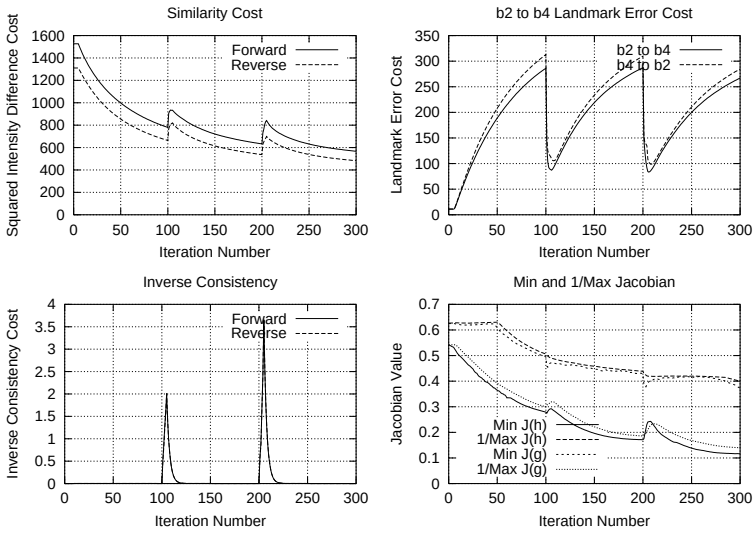

Figure 11: Plots of the intensity and landmark costs as a function of iteration for the CLI-TPS registration of data-sets $B2$ and $B4$.

Table 3 also demonstrates that the CI-TPS and CLI-TPS registrations have a smaller average intensity difference, but larger fiducial landmark errors. The CLI-TPS has smaller average intensity difference and smaller fiducial landmark errors than the CI-TPS registration algorithm. The CLI-TPS algorithm produces a better similarity match because the landmark driving force pulls the intensity driving function out of local minima. It should be noted that the large number of landmarks used in the CLI-TPS registration limits the effect of the intensity driving force in neighborhoods of the landmarks. In practice, when the the landmark points are more sparse the intensity driving force plays a more important role.

4 Summary and Conclusions

This work presented two new image registration algorithms based on thin-plate spline regularization: landmark-based consistent thin-plate spline (CL-TPS) image registration and landmark and intensity-based consistent thin-plate spline image registration (CLI-TPS). It was shown that the inverse consistency error between the forward and reverse transforma-

tions generated from the traditional unidirectional thin-plate spline algorithm(UL-TPS) could be minimized using the CL-TPS algorithm. Inverse consistency error images showed that the largest error occurred away from the landmark points for the UL-TPS algorithm and near the landmark points for the CL-TPS algorithm. The maximum CL-TPS inverse consistency error was reduced by 500 times in the inner-to-outer dots example and greater than 6 times in the MRI brain example when compared with the UL-TPS registration. The Jacobian error was reduced from 1.4 to 0.0012 for the inner-to-outer dots example and from 0.050 to 0.034 for the MRI brain example. Using landmark and intensity information with the MRI brain example gave a better intensity matching between the images than just using the landmark information as visualized in Fig. 8 and by a decrease in the average intensity difference recorded in table 3. It was shown that using both landmark and intensity information gave a better registration of the MRI brain images than using the intensity or landmark information alone.

Acknowledgments

We would like to thank John Haller and Michael W. Vannier of the Department of Radiology, The University of Iowa for providing the MRI data. This work was supported in part by the NIH grant NS35368 and a grant from the Whitaker Foundation.

Table 3: Experimental results produced by mapping MRI brain image 2 into images 1, 3, 4, and 5 (see Fig. 7). The thin-plate spline algorithms compared in this table are the unidirectional landmark (UL-TPS), averaged unidirectional landmark (AUL-TPS), consistent landmark (CL-TPS), consistent intensity (CI-TPS), and consistent landmark and intensity (CLI-TPS) algorithms. The statistics computed for these experiments were the average fiducial error (AFE) in pixels, maximum fiducial error (MFE), maximum inverse error (MIE) in pixels, average inverse error (AIE) in pixels, masked average intensity difference (MAID), minimum Jacobian value (MJ), inverse of the maximum Jacobian value (IJ) and the Jacobian error (JE).

Algorithm	Exp.	AFE	MFE	AIE	MIE	MAID	MJ	IJ	JE
None	b2b1	6.9	12			0.23			
	b2b3	4.9	13			0.19			
	b2b4	8.8	21			0.22			
	b2b5	8.7	19			0.26			
UL-TPS	b2b1	0.066	0.087	0.90	2.7	0.16	0.56	0.75	0.053
	b2b3	0.073	0.098	0.78	3.1	0.18	0.50	0.57	0.092
	b2b4	0.062	0.088	0.94	3.4	0.13	0.51	0.66	0.090
	b2b5	0.030	0.061	1.2	3.8	0.16	0.56	0.67	0.050
AUL-TPS	b2b1	0.016	0.029	0.0057	0.13	0.16	0.59	0.73	0.00048
	b2b3	0.017	0.053	0.0066	0.10	0.18	0.55	0.53	0.0023
	b2b4	0.030	0.065	0.0096	0.22	0.13	0.54	0.62	0.0010
	b2b5	0.031	0.046	0.0096	0.12	0.16	0.56	0.62	0.0011
CL-TPS	b2b1	0.000030	0.00011	0.0012	0.028	0.16	0.59	0.73	0.0011
20 iter.	b2b3	0.000034	0.00014	0.0016	0.022	0.18	0.55	0.53	0.0014
	b2b4	0.0083	0.083	0.079	0.42	0.13	0.54	0.62	0.0011
	b2b5	0.000006	0.00037	0.0024	0.015	0.16	0.56	0.62	0.00021
CI-TPS	b2b1	1.5	3.1	0.0045	0.048	0.097	0.26	0.47	0.011
1000 iter.	b2b3	1.6	2.9	0.0043	0.052	0.11	0.25	0.29	0.017
	b2b4	1.0	2.2	0.0040	0.063	0.084	0.26	0.44	0.0075
	b2b5	1.4	3.4	0.0044	0.099	0.092	0.18	0.32	0.0091
CLI-TPS	b2b1	1.1	2.0	0.020	0.40	0.091	0.19	0.37	0.036
300 iter.	b2b3	1.1	2.0	0.021	0.62	0.10	0.13	0.23	0.030
	b2b4	0.75	1.6	0.017	0.61	0.080	0.12	0.39	0.025
	b2b5	1.1	2.8	0.021	0.96	0.088	0.10	0.17	0.034

References

[1] F.L. Bookstein. *The Measurement of Biological Shape and Shape Change*, volume 24. Springer-Verlag: Lecture Notes in Biomathematics, New York, 1978.

[2] F.L. Bookstein. Linear methods for nonlinear maps: Procrustes fits, thin-plate splines, and the biometric analysis of shape variability. In Toga [18], pages 157–181.

[3] F.L. Bookstein and W.D.K. Green. Edge information at landmarks in medical images. In Richard A. Robb, editor, *Visualization in Biomedical Computing 1992*, pages 242–258. SPIE 1808, 1992.

[4] Fred L. Bookstein. *Morphometric Tools for Landmark Data*. Cambridge University Press, New York, 1991.

[5] G.E. Christensen. Consistent linear-elastic transformations for image matching. In A. Kuba and M. Samal, editors, *Information Processing in Medical Imaging*, LCNS 1613, pages 224–237. Springer-Verlag, June 1999.

[6] G.E. Christensen and H.J. Johnson. Consistent image registration. *IEEE Transactions on Medical Imaging*, 20(7):568–582, July 2001.

[7] I.L. Dryden and K.V. Mardia. *Statistical Shape Analysis*. Wiley, 1998.

[8] A.C. Evans, C. Beil, S. Marret, C.J. Thompson, and A. Hakim. Anatomical-functional correlation using an adjustable MRI-based region of interest atlas with positron emission tomography. *Journal of Cerebral Blood Flow and Metabolism*, 8:513–530, 1988.

[9] U. Grenander and M. I. Miller. Computational anatomy: An emerging discipline. *Quarterly of Applied Mathematics*, LVI(4):617–694, December 1998.

[10] Hans J. Johnson. Method for consistent linear-elastic medical image registration. Master's thesis, Department of Electrical and Computer Engineering, The University of Iowa, Iowa City, IA 52242, May 2000.

[11] S.C. Joshi. *Large deformation diffeomorphisms and Gaussian random fields for statistical characterization of brain sub-manifolds*. D.Sc. Dissertation, Department of Electrical Engineering, Sever Institute of Technology, Washington University, St. Louis, MO. 63130, Dec 1997.

[12] S.C. Joshi and M. I. Miller. Landmark matching via large deformation diffeomorphisms. *IEEE Transactions on Image Processing*, 9(8):1357–1370, August 2000.

[13] S.C. Joshi, M.I. Miller, G.E. Christensen, A. Banerjee, T.A. Coogan, and U. Grenander. Hierarchical brain mapping via a generalized Dirichlet solution for mapping brain manifolds. In R.A. Melter, A.Y. Wu, F.L. Bookstein, and W.D. Green, editors, *Vision Geometry IV*, Proceedings of SPIE Vol. 2573, pages 278–289, 1995.

[14] J.T. Kent and K.V. Mardia. The link between kriging and thin-plate splines. In F.P. Kelly, editor, *Probability, Statistics and Optimisation*. John Wiley and Sons, 1994.

[15] M.I. Miller, S.C. Joshi, and G.E. Christensen. Large deformation fluid diffeomorphisms for landmark and image matching. In Toga [18], pages 115–132.

[16] K. Rohr, M. Fornefett, and H.S. Stiehl. Approximating thin-plate splines for elastic registration: Integration of landmark errors and orientation attributes. In A. Kuba and M. Samal, editors, *Information Processing in Medical Imaging*, LCNS 1613, pages 252–265. Springer-Verlag, June 1999.

[17] J. Talairach and P. Tournoux. *Co-Planar Stereotactic Atlas of the Human Brain*. Beorg Thieme Verlag, Stuttgart, 1988.

[18] A. Toga, editor. *Brain Warping*. Academic Press, San Diego, 1999.

A Estimating Thin-plate Spline Parameters

The unknown UL-TPS parameters $W = [\xi_1, \ldots, \xi_M, a_1, a_2, b]^T$ in Eq. 3 are determined by solving the linear system of equations that result by fixing the displacement field values

at landmark locations. Let $\phi_{i,j} = \phi(|p_i - p_j|)$ and build the matrix

$$K = \begin{bmatrix} \Phi & \Lambda \\ \Lambda^T & O \end{bmatrix} \quad where \quad \Phi = \begin{bmatrix} \phi_{1,1} & \phi_{1,2} & \dots & \phi_{1,M} \\ \phi_{2,1} & \phi_{2,2} & \dots & \phi_{2,M} \\ \vdots & \vdots & \ddots & \vdots \\ \phi_{M,1} & \phi_{M,2} & \dots & \phi_{M,M} \end{bmatrix}, \quad \Lambda = \begin{bmatrix} p_1 & q_1 & 1 \\ p_2 & q_2 & 1 \\ \vdots & \vdots & \vdots \\ p_M & q_M & 1 \end{bmatrix}, \tag{5}$$

where O is a 3×3 matrix of zeros. Also, define the $(M+3) \times 2$ matrix of landmark displacements as $D = [d_1, \dots, d_M, 0, 0, 0]^T$ where $d_i = q_i - p_i$ for $i = 1, \dots, M$. The equations formed by substituting the landmark constrains into Eq. 3 can be written in matrix form as $D = KW$. The solution W to this matrix equation is determined by least squares estimation since the matrix K is not guaranteed to be full rank.

B Consistent Intensity-based Registration

The consistent intensity-based registration (CI-TPS) algorithm [5, 6, 10] using thin-plate spline regularization is briefly described here. It is based on minimizing the cost function given by

$$\begin{aligned} C &= \sigma \int_\Omega |T(h(x)) - S(x)|^2 + |S(g(x)) - T(x)|^2 dx \\ &+ \rho \int_\Omega ||\mathcal{L}u(x)||^2 + ||\mathcal{L}w(x)||^2 dx + \chi \int_\Omega ||u(x) - \tilde{w}(x)||^2 + ||w(x) - \tilde{u}(x)||^2 dx \end{aligned} \tag{6}$$

The intensities of T and S are assumed to be scaled between 0 and 1. The first integral of the cost function defines the cumulative squared error similarity cost between the transformed template $T(h(x))$ and target image $S(x)$ and between the transformed target $S(g(y))$ and the template image $T(y)$. To use this similarity function, the images T and S must correspond to the same imaging modality and they may require pre-processing to equalize the intensities of the image. The similarity function defines the correspondence between the template and target images as the forward and reverse transformations h and

g, respectively, that minimize the squared error intensity differences between the images. The second integral is used to regularize the forward and reverse displacement fields u and w, respectively. This term is used to enforce the displacement fields to be smooth and continuous. The third integral is called the inverse consistency constraint and is minimized when the forward and reverse transformations h and g, respectively, are inverses of each other. The constants σ, ρ, and χ define the relative importance of each term of the cost function.

The cost function in Eq. 7 is discretized to numerically minimize it. The forward and reverse transformations h and g and their associated displacement fields u and w are parameterized by the discrete Fourier series defined by

$$u_d[n] = \sum_{k \in \Omega_d} \mu[k] e^{j<n,\theta[k]>} \quad \text{and} \quad w_d[n] = \sum_{k \in \Omega_d} \eta[k] e^{j<n,\theta[k]>} \tag{7}$$

for $n \in \Omega_d$ where the basis coefficients $\mu[k]$ and $\eta[k]$ are (2×1) complex-valued vectors and $\theta[k] = [\frac{2\pi k_1}{N_1}, \frac{2\pi k_2}{N_2}]^T$. The basis coefficients have the property that they have complex conjugate symmetry, i.e., $\mu[k] = \mu^*[N-k]$ and $\eta[k] = \eta^*[N-k]$. The notation $< \cdot, \cdot >$ denotes the dot product of two vectors such that $< n, \theta[k] >= \frac{2\pi k_1 n_1}{N_1} + \frac{2\pi k_2 n_2}{N_2}$. The basis coefficients $\mu[k]$ and $\eta[k]$ of the discretized forward and reverse displacement fields are then minimized using gradient descent as described in [5, 6].

The intensity similarity component of the cost function is forced to register the global intensity patterns before local intensity patterns by restricting the similarity gradient to modify only the low frequencies of the displacement field parameters. Restricting the similarity cost gradient to modifying the low frequency components is analogous to filtering with a zonal low-pass filter. To mitigate the Gibbs ringing associated with zonal low-pass filters, a low-pass Butterworth filter is applied to the similarity cost gradient in the gradient decent algorithm.